Quantum Quasi-Monte Carlo Technique for Many-Body Perturbative Expansions

Marjan Maček[1], Philipp T. Dumitrescu[2,*], Corentin Bertrand[2], Bill Triggs[3],
Olivier Parcollet[2,4], and Xavier Waintal[1,†]

[1]*Université Grenoble Alpes, CEA, IRIG-PHELIQS, 38000 Grenoble, France*
[2]*Center for Computational Quantum Physics, Flatiron Institute, 162 5th Avenue, New York, New York 10010, USA*
[3]*Laboratoire Jean Kuntzmann, Université Grenoble Alpes, CNRS, 38401 Grenoble, France*
[4]*Université Paris-Saclay, CNRS, CEA, Institut de physique théorique, 91191 Gif-sur-Yvette, France*

High order perturbation theory has seen an unexpected recent revival for controlled calculations of quantum many-body systems, even at strong coupling. We adapt integration methods using low-discrepancy sequences to this problem. They greatly outperform state-of-the-art diagrammatic Monte Carlo simulations. In practical applications, we show speed-ups of several orders of magnitude with scaling as fast as $1/N$ in sample number N; parametrically faster than $1/\sqrt{N}$ in Monte Carlo simulations. We illustrate our technique with a solution of the Kondo ridge in quantum dots, where it allows large parameter sweeps.

The exponential complexity of quantum many-body systems is at the heart of many remarkable phenomena. Advances in correlated materials and recently developed synthetic quantum systems—e.g., atomic gases [1], trapped ions [2], and nanoelectronic devices [3–6]—have allowed many-body states to be characterized and controlled with unprecedented precision. The latest of these systems, quantum computing chips, are highly engineered out-of-equilibrium many-body systems, where the interacting dynamics performs computational tasks [7]. However, our understanding of these many-body systems is limited by their intrinsic complexity. While uncontrolled approximations can give insight into possible behaviors, there is a growing effort to develop controlled, high-precision methods [8], especially ones that apply far from equilibrium [9–11]. These allow us to make quantitative predictions about the physics of many-body systems and to uncover qualitatively new effects at strong coupling.

Among theoretical approaches, perturbative expansions in the interaction strength have seen an unexpected recent revival, in particular using a family of "diagrammatic" quantum Monte Carlo methods (DiagQMC) [10–21]. Using various techniques [11,12,18,21], it is now possible to sum perturbative series beyond their radius of convergence and thus access strongly correlated regimes. The effects of strong interactions have been studied in diverse systems, including unitary quantum gases [15], polarons [12], quantum dots [10,11,19], and pseudogap metals [16].

DiagQMC is currently the preferred strategy for computing series coefficients at large perturbation order n, as this involves integrals of dimension proportional to n (practically around 5–30). High dimensional integration is notoriously difficult, and Monte Carlo simulations

provide a robust and flexible solution with errors that scale as $1/\sqrt{N}$ independently of the dimension; here N is the number of sample points.

Nonetheless, there has been tremendous progress in integration methods for problems that lie in between traditional quadrature (very low dimensions) and Monte Carlo methods (high dimensions). In intermediate dimensions (typically 5–200), "quasi-Monte Carlo" methods have become well established. These sample the integrand in a deterministic and structured way that ensures improved uniformity and better convergence rates. In favorable cases they can achieve error scalings of $1/N$ or even $1/N^2$, far outperforming traditional Monte Carlo methods [22–25].

In this Letter we show how to apply these integration techniques to perturbative expansions for quantum many-body systems. Our "quantum quasi-Monte Carlo" method (QQMC) is broadly applicable. It can be formulated for both equilibrium and nonequilibrium cases and extended to various lattices and dimensions. Here we demonstrate it on a quantum dot model and show computational accelerations of several orders of magnitude compared to state-of-the-art DiagQMC [10,11] (Fig. 1). A crucial ingredient of the QQMC is the *warping* of the integral. This is a multidimensional change of variables constructed from a model function that approximates the integrand. We show that a simple model already yields remarkable results and propose directions for future optimizations. We demonstrate convergence as fast as $1/N$ in a high-precision benchmark against an exact Bethe ansatz solution, to order $n = 12$. To illustrate the power of QQMC methods, we calculate the finite-bias current through a quantum dot in the Kondo regime, sweeping electrostatic gating and
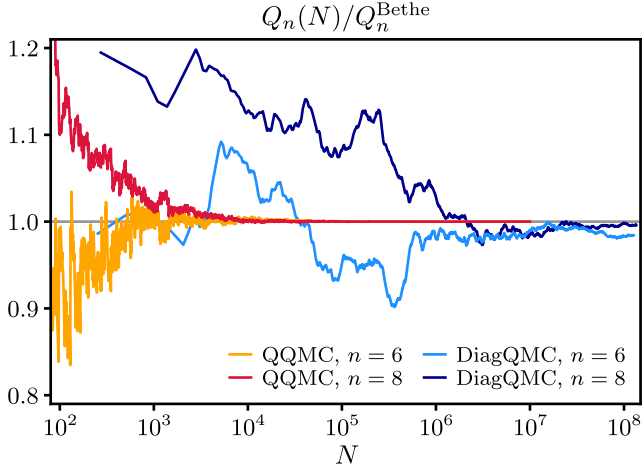
FIG. 1. Comparison of the convergence rates for QQMC and DiagQMC. Here $Q_n(N)$ is the expansion coefficient of the occupation number of the Anderson impurity model at order n as a function of the number of integrand evaluations N. Each result is normalized to the exact analytic result Q_n^{Bethe}.

interaction strength as parameters. This experimentally relevant calculation was computationally unfeasible for previous techniques.

Formalism.—In perturbative calculations, an observable $F(U)$ such as a current or susceptibility is expressed as a power series in the interaction U:

$$F(U) = \sum_{n=0}^{\infty} F_n U^n, \qquad (1)$$

where the coefficients F_n are n-dimensional integrals

$$F_n = \int d^n u \, f_n(u_1, u_2, \ldots, u_n). \qquad (2)$$

The integrands $f_n(u)$ are time-ordered correlators expressed in terms of 2^n determinants (Wick's theorem), in both Schwinger-Keldysh [10] and Matsubara formalisms [17]. The exponential complexity of evaluating $f_n(u)$ leads us to seek fast integration methods. Here the u_i specify the locations of interaction vertices in space and time. We present the formalism generally and will specialize to a concrete application later.

We will perform the integral Eq. (2) by direct sampling using quasi-Monte Carlo simulations. The crucial step is to warp the integral, i.e., to make a change of variables $u(x)$ that maps the hypercube $x \in [0,1]^n$ onto the u domain. The integral Eq. (2) becomes

$$F_n = \int_{[0,1]^n} d^n x \, f_n[u(x)] \left| \frac{\partial u}{\partial x} \right|, \qquad (3)$$

where $|\partial u/\partial x|$ is the associated Jacobian.

The most important property of the warping is to make the function $\bar{f}_n(x) = f_n[u(x)]|\partial u/\partial x|$ as smooth as possible in the new variables x. If f_n were positive, the perfect change of variables would make $\bar{f}_n$ constant and thus trivial to integrate with a single sample. That would be tantamount to ideal sampling from the distribution $f_n(u)$ and it is as challenging as the original integration. Instead, a judicious warping must provide sufficient smoothing while remaining efficiently computable.

Mathematically, convergence theorems can only be established for $\bar{f}_n(x)$ that belong to specific smooth function spaces, or whose Fourier coefficients have rapid asymptotic decay properties [22,24]. Although we cannot prove that our warped integrands satisfy assumptions of this kind, in practice we find that the change of variables are good enough to provide excellent error scaling.

To warp the integral, we consider a positive model function $p_n(u)$, which should be viewed as an approximation of $|f_n|$. The inverse change of variables $x(u)$ is then defined by (for $1 \leq m \leq n$),

$$x_m(u'_m, u_{m+1}, \ldots, u_n) = \frac{\int_0^{u'_m} du_m \int_0^{\infty} \prod_{i=1}^{m-1} du_i \, p_n(u)}{\int_0^{\infty} du_m \int_0^{\infty} \prod_{i=1}^{m-1} du_i \, p_n(u)}. \qquad (4)$$

Here we adopt a case where u_i is defined on the interval $[0, \infty)$. Since $x_m(u)$ only depends on $u_m, \ldots, u_n$, the Jacobian is $|\partial u/\partial x| = [\int du \, p_n(u)]/p_n(u)$ (see Ref. [26]). In quasi-Monte Carlo simulations, the integral Eq. (3) is approximated by a sum over the first N points of a low-discrepancy sequence $\bar{x}_i$. This is a deterministic sequence of points with specific properties that uniformly samples the hypercube [22,24]. We have

$$F_n \approx F_n(N) = \frac{\mathcal{C}}{N} \sum_{i=0}^{N} \frac{f_n[u(\bar{x}_i)]}{p_n[u(\bar{x}_i)]}, \qquad (5)$$

where $\mathcal{C} = \int du \, p_n(u)$ is a constant. Here we use a Sobol' sequence [47,48] to obtain $\bar{x}_i$.

The model function $p_n(u)$ should have two key properties. First, it should approximate $|f_n(u)|$ well. Second, its form should be simple enough for the partial integrals Eq. (4) to be evaluated exactly and quickly. This allows the reciprocal function $u(x)$ to be computed by first inverting the one-dimensional function $x_n(u_n)$, then inverting $x_{n-1}(u_n, u_{n-1})$ for fixed u_n, and so on [26].

Many classes of model functions are possible, as discussed later. This Letter applies the method to impurity models, using a real-time Schwinger-Keldysh formalism, in which the u_i are the times of the interaction vertices. We consider the simple form

$$p_n(u) = \prod_{i=1}^{n} h^{(i)}(u_{i-1} - u_i), \qquad (6)$$

with $0 < u_n < u_{n-1} < \dots < u_1 < u_0$. Here $u_0 = t$ is defined to be the measurement time and the $h^{(i)}$ are positive scalar functions. (They may depend on n, but we omit this index.) The factored structure allows Eq. (4) to be inverted rapidly [26].

Anderson impurity.—We illustrate our method on the Anderson impurity model coupled to two leads. This is the canonical model for a quantum dot with Coulomb repulsion and the associated Kondo effect. It has been realized in many nanoelectronic experiments [3–6]. Importantly, some quantities including the electron occupation on the dot Q can be computed analytically in the universal limit with the Bethe ansatz [49,50]. This provides us with a high-precision benchmark for QQMC at any perturbation order n.

We consider an infinite one-dimensional chain with the impurity at site $i = 0$. The noninteracting Hamiltonian is $H_0 = \sum_{i,\sigma}(\gamma_i c_{i,\sigma}^\dagger c_{i+1,\sigma} + \text{H.c.}) + \varepsilon_d \sum_\sigma c_{0\sigma}^\dagger c_{0\sigma}$, where $\sigma = \uparrow, \downarrow$ is the electronic spin and ε_d represents a capacitive gate coupled to the dot. The local Coulomb repulsion is $H_{\text{int}} = U c_{0\uparrow}^\dagger c_{0\uparrow} c_{0\downarrow}^\dagger c_{0\downarrow}$. The electron tunneling between the leads and dot is $\gamma_0 = \gamma_{-1} = \gamma$. All other $\gamma_i = D/2$, corresponding to hopping within the leads; the lead half-bandwidth D is a constant. We perform the perturbative expansion in powers of U [26].

Benchmark.—To validate the QQMC method, we consider the special case solved by the Bethe ansatz. For this, we set temperature $T = 0$, capacitive gate $\varepsilon_d = 0$, and half-bandwidth $D \to +\infty$ such that $\Gamma = 4\gamma^2/D = 1$ is the unit of energy. The measurement time $t = 30/\Gamma$ is sufficiently long that the system reaches steady state. We compute the expansion of the occupation number $Q(U) = \langle c_{0\uparrow}^\dagger c_{0\uparrow} + c_{0\downarrow}^\dagger c_{0\downarrow} \rangle$. The system is particle-hole symmetric for $\varepsilon_d = -U/2$ so the non-interacting case is $Q_0 = 1$. For higher-order Q_n, particle-hole symmetry is broken, but the expansion stays in the symmetric regime $(U + 2\varepsilon_d) \ll \sqrt{U\Gamma}$ [49].

Figure 2 shows the relative error between $Q_n(N)$ using QQMC and the exact result Q_n^{Bethe} [26], as a function of the number of integrand evaluations N. Following an initial transient, we enter an asymptotic regime in which there is rapid convergence: for $n = 4$ this is consistent with pure $1/N$ while for $n = 8, 12$ it is $1/N^\delta$ with $\delta \simeq 0.9, 0.8$. These calculations used the product model function Eq. (6) with a single exponential $h^{(i)}(v_i) = \exp(-v_i/\tau)$, where $\tau = 0.95$. The same setup was used in Fig. 1. The level of precision that we obtained revealed limitations in the conventional evaluation of the noninteracting Green functions, which warranted special consideration [26].

It is expected that the convergence rate gradually slows as n increases. First, the quality of the warping decreases as the disparity between the increasingly severe requirements of convergence theory and the behavior of our integrands grows. This can be mitigated by constructing more expressive model functions, which we discuss below. Second, for
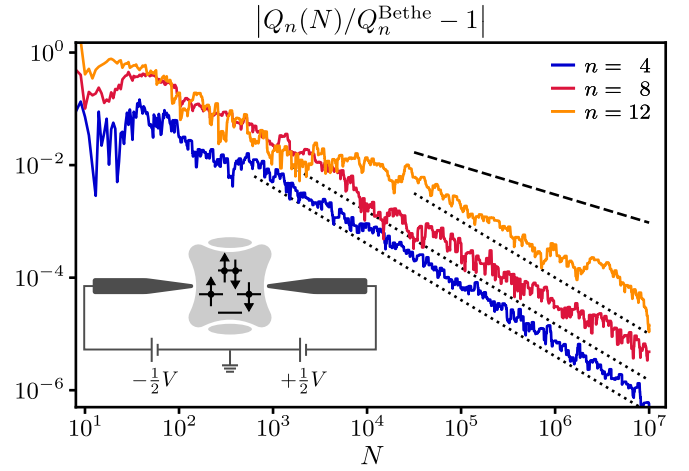

FIG. 2. Expansion coefficients Q_n for the Anderson impurity occupation number relative to the analytic result Q_n^{Bethe}. QQMC methods converge at rates close to $1/N$ with the number of integrand evaluations N. For visibility, the data have been smoothed (see Supplemental Material [26]). The black lines indicate exact $1/N$ (dotted) and $1/\sqrt{N}$ (dashed) convergence. Each run was performed with one Sobol' sequence. Inset: Cartoon of quantum dot setup.

larger n the integrands generally become more oscillatory. The model functions Eq. (4) were not designed to handle cases with massive cancellation, and this may become a limiting factor. We will see this effect below for calculations with $\varepsilon_d/U > 0.5$, although in practice enough orders can be computed accurately to obtain the desired physical results [26].

In quasi-Monte Carlo methods, a standard technique to estimate errors is to perform computations using Eq. (5) with several "randomized" low-discrepancy sequences [22–25] and we use this method below [26].

Having made these technical points, let us reiterate the lessons of Figs. 1 and 2: (i) QQMC provide a dramatic speed-up with better asymptotic error scaling than DiagQMC; (ii) the speed-up persists to at least order $n = 12$, which is what is needed for practical applications.

Coulomb diamond.—We now apply QQMC to solve a topical physics problem. We explore the current-voltage characteristic $I(V)$ across the quantum dot for finite bias and varying U. Since quantum dots are considered promising platforms for building qubit systems, it is of primary importance to understand how many-body effects influence their properties, especially the phase coherence.

Quantum dots can be in three different experimentally accessible regimes [51–54]: Fabry-Pérot (small U), Kondo (intermediate U), and Coulomb blockade (large U). The Fabry-Pérot and Coulomb blockade limits are well described by, respectively, noninteracting and semiclassical theories; the out-of-equilibrium Kondo regime is more challenging. Two controlled approaches have recently appeared, but both are too slow for some applications:
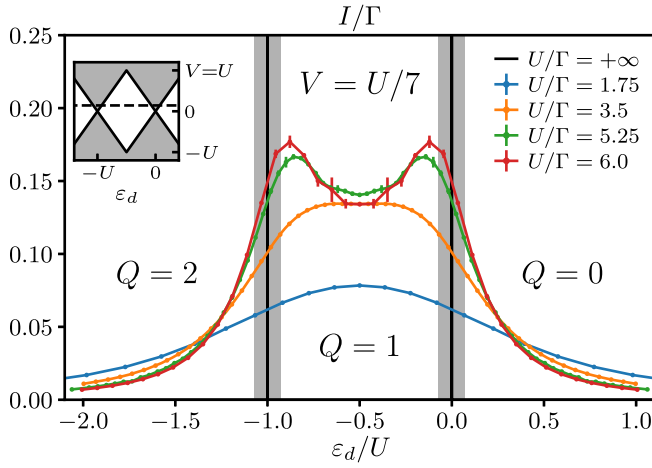
FIG. 3. Current at finite-bias voltage through the Anderson impurity at $T = 0$, sweeping through several interaction regimes. Each point is a different QQMC calculation up to order $n = 10$, including series resummation [11]. The error bars are a combination of integration error and truncation error of the resummation; the latter dominates. By construction, the data are symmetric with respect to the particle-hole symmetric point $\varepsilon_d = -U/2$. Inset: Coulomb diamond in the Coulomb blockade picture (large U). Regions where current can flow are shaded gray. The dashed line indicates the scan shown in the main plot (varying ε_d for fixed $V/U = 1/7$).

FIG. 4. Comparison of convergence of Q_8 for different methods of integration: evaluating unwarped integrand with a Sobol' sequence (cyan), DiagQMC (red), warped integral sampled with Mersenne Twister pseudorandom numbers (green), or Sobol' sequence (blue). For the warped cases, we used Eq. (6) with $h^{(i)}(v_i) = \exp(-v_i/\tau), \tau = 0.95$. After an initial warping with exponential functions $\tau = 1.1$, we can apply an additional warping obtained by projection (orange) [26]. For visibility, the data (except Sobol' and DiagQMC) have been smoothed in the same way as in Fig. 2.

the Schwinger-Keldysh DiagQMC used in Figs. 1 and 4 [10,11] and the real-time inchworm algorithm [9,55,56]. QQMC provide the speed and precision to allow large parameter sweeps, which is mandatory to make good contact with experiments. In Ref. [11], some of us studied the Kondo ridge close to $\varepsilon_d = -U/2$. QQMC allow us to present results scanning the entire (U, ε_d) phase diagram, including slowly converging regions with even numbers of electrons or near the degeneracy points.

Figure 3 (inset) shows a cartoon of the differential conductance for varying (ε_d, V) as predicted by Coulomb blockade theory [57] and seen experimentally at low temperatures and large U [58]. At small bias, the Coulomb blockade forbids current flows except at two special points: $\varepsilon_d = 0$, where the dot energies for $Q = 0$ and $Q = 1$ electrons are degenerate, and $\varepsilon_d = -U$ (likewise for $Q = 1, 2$). At intermediate U, the Kondo effect changes this picture drastically: the zero-bias Kondo resonance forms in the "forbidden" region of odd Q and enables current flow.

Figure 3 shows the current I versus gate voltage ε_d for $V = U/7$ and temperature $T = 0$. We choose a finite half-bandwidth $D/\Gamma = 20$ [26]. Sweeping the interaction U/Γ shows several regimes. For $U/\Gamma = 1.75$, 3.5 a current plateau emerges in the local moment regime ($Q = 1$) due to Kondo resonance formation. The current develops new local maxima seen for $U/\Gamma = 5.25$, 6.00. These grow toward the Coulomb blockade limit at larger U (black
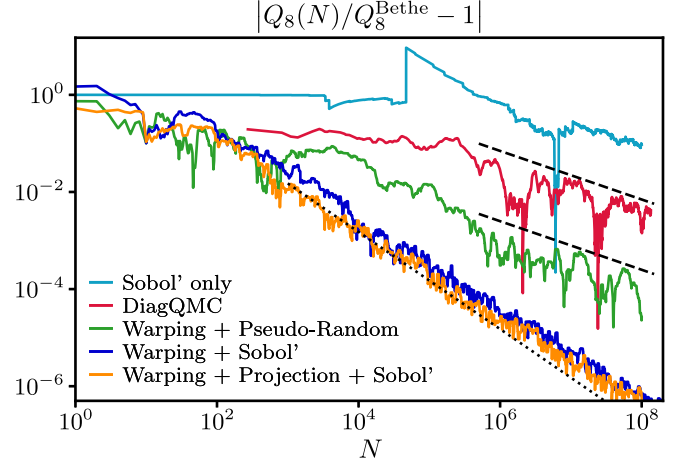
lines); at the same time, current around $\varepsilon_d/U = -0.5$ reaches a maximum and decreases. This is a competition between resonance formation and narrowing. At small U, the Kondo temperature T_K is much larger than the bias V and we are in the linear response regime. In this regime near $\varepsilon_d = -U/2$ we approach perfect transmission $I = V/\pi$; see Ref. [11]. At larger $U \gtrsim 4\Gamma$, T_K decreases exponentially with U and become smaller than V, leaving the linear response regime. Throughout, as U increases, the already-small current in the side regions ($Q = 0, 2$) is increasingly suppressed.

Model function.—Let us reexamine the importance of integral warping and model functions. Figure 4 shows the convergence of $Q_8(N)$ using different integration methods; the parameters are identical to Fig. 2. When the integral is evaluated using Sobol' points without warping ("Sobol' only") the convergence is poor, showing that naively applying low-discrepancy sequences provides little benefit for these integrands. Next, contrast regular DiagQMC methods with the warped integrand using pseudorandom numbers. As expected for pure Monte Carlo approaches, both show $1/\sqrt{N}$ convergence. Nonetheless, sampling the warped integrand still converges faster than the DiagQMC, despite the fact that the latter uses importance sampling via the Metropolis algorithm. As anticipated, QQMC using Sobol' points and the model function Eq. (6) based on exponential $h^{(i)}$ converge even more rapidly.

How can the model function Eq. (6) with simple $h^{(i)}$ provide such dramatic convergence improvements? Our

integrands describe physical correlators that are highly structured and have decaying exponential or power-law tails [10,19,26]. The tail contributions become ever more important as the dimension increases. The model function properly describes the long-time asymptotics [26]. We also emphasize the importance of a well-chosen coordinate system in the model function: the differences of closest times $v_i = u_{i-1} - u_i$ used to parametrize the $h^{(i)}$.

Optimization of the model function should allow further performance gains, particularly at higher orders n. One possibility is to better adapt the functions $h^{(i)}$ to f_n. To illustrate this, we apply a second warping constructed by sampling points from the first warping. These samples are projected along the dimensions of v space and smoothed [26]. As shown in Fig. 4, this optimization reduces the error by a factor of $\simeq 2$. More importantly, it automatically gives robust convergence without the need to manually optimize the τ parameter [26].

Finally, other families of model functions exist beyond Eq. (6), that provide versatile and expressive approximations while still allowing for fast inversion of Eq. (4). One such family is matrix product states (MPS) or functional tensor-trains [59,60], of which Eq. (6) is just the simplest case:

$$p_n(\boldsymbol{u}) = h_a^{(1)}(v_1) h_{ab}^{(2)}(v_2) \cdots h_{cd}^{(n-1)}(v_{n-1}) h_d^{(n)}(v_n). \quad (7)$$

Here, $h_{ab}^{(i)}$ are matrices and repeated indices are summed. Another promising family is $p_n(\boldsymbol{u}) = \prod_{i=1}^{n-1} \bar{h}^{(i)}(v_{i+1}, v_i)$.

Conclusion.—We have shown how to use sampling techniques based on low-discrepancy sequences to compute high orders of many-body perturbation theory. Although we cannot show that the integrands obey the assumptions of formal quasi-Monte Carlo convergence theory, practical scaling as fast as $1/N$ is still achievable. This success was possible due to the warping of the integral based on a model function. Using benchmarks on exactly solvable quantities in the Anderson impurity model, we unambiguously validated the convergence of this quantum quasi-Monte Carlo method at high precision. This calculation was about $\sim 10^4$ times faster than the DiagQMC equivalent.

We can apply the techniques established here to models with interesting strongly correlated physics in all dimensions, for equilibrium and especially nonequilibrium situations. For continuum models, the integrands are smooth and warping should be particularly simple. For lattice models, the discrete summation may degrade convergence, although this may be addressed with sufficiently good model functions. QQMC can also be applied to other diagrammatic expansions, e.g., in hybridization [9]. Constructing more expressive model functions should further increase speed and accuracy and is an ideal application for recent machine learning techniques in quantum systems.

Finally, we have shown in our calculations that the simple model function Eq. (6) captures the behavior of perturbation theory integrands in asymptotic large-coordinate regions. This is not accidental, but reveals a simplifying structure of the correlation functions arising from Wick's theorem that was not previously appreciated in diagrammatic numerical simulations. For the real-time Schwinger-Keldysh calculations, the contour index means that the MPS structure Eq. (7) is the natural approximation for generic many-body systems. It can be used as a starting point to efficiently compute and integrate these functions, even beyond the Monte Carlo or QQMC sampling discussed here.

*pdumitrescu@flatironinstitute.org
†xavier.waintal@cea.fr

[1] C. Gross and I. Bloch, Quantum simulations with ultracold atoms in optical lattices, Science 357, 995 (2017).
[2] R. Blatt and C. F. Roos, Quantum simulations with trapped ions, Nat. Phys. 8, 277 (2012).
[3] D. Goldhaber-Gordon, H. Shtrikman, D. Mahalu, D. Abusch-Magder, U. Meirav, and M. A. Kastner, Kondo effect in a single-electron transistor, Nature (London) 391, 156 (1998).
[4] D. Goldhaber-Gordon, J. Göres, M. A. Kastner, H. Shtrikman, D. Mahalu, and U. Meirav, From the Kondo Regime to the Mixed-Valence Regime in a Single-Electron Transistor, Phys. Rev. Lett. 81, 5225 (1998).
[5] S. M. Cronenwett, T. H. Oosterkamp, and L. P. Kouwenhoven, A tunable Kondo effect in quantum dots, Science 281, 540 (1998).
[6] Z. Iftikhar, A. Anthore, A. K. Mitchell, F. D. Parmentier, U. Gennser, A. Ouerghi, A. Cavanna, C. Mora, P. Simon, and F. Pierre, Tunable quantum criticality and super-ballistic transport in a "charge" Kondo circuit, Science 360, 1315 (2018).
[7] H. Bernien, S. Schwartz, A. Keesling, H. Levine, A. Omran, H. Pichler, S. Choi, A. S. Zibrov, M. Endres, M. Greiner, V. Vuletić, and M. D. Lukin, Probing many-body dynamics on a 51-atom quantum simulator, Nature (London) 551, 579 (2017).
[8] J. P. F. LeBlanc et al. (Simons Collaboration on the Many-Electron Problem), Solutions of the Two-Dimensional Hubbard Model: Benchmarks and Results from a Wide Range of Numerical Algorithms, Phys. Rev. X 5, 041041 (2015).
[9] G. Cohen, E. Gull, D. R. Reichman, and A. J. Millis, Taming the Dynamical Sign Problem in Real-Time

Evolution of Quantum Many-Body Problems, Phys. Rev. Lett. **115**, 266802 (2015).

[10] R. E. V. Profumo, C. Groth, L. Messio, O. Parcollet, and X. Waintal, Quantum Monte Carlo for correlated out-of-equilibrium nanoelectronic devices, Phys. Rev. B **91**, 245154 (2015).

[11] C. Bertrand, S. Florens, O. Parcollet, and X. Waintal, Reconstructing Nonequilibrium Regimes of Quantum Many-Body Systems from the Analytical Structure of Perturbative Expansions, Phys. Rev. X **9**, 041008 (2019).

[12] N. V. Prokof'ev and B. V. Svistunov, Polaron Problem by Diagrammatic Quantum Monte Carlo, Phys. Rev. Lett. **81**, 2514 (1998).

[13] N. V. Prokof'ev and B. V. Svistunov, Bold diagrammatic Monte Carlo: A generic sign-problem tolerant technique for polaron models and possibly interacting many-body problems, Phys. Rev. B **77**, 125101 (2008).

[14] A. S. Mishchenko, N. V. Prokof'ev, B. V. Svistunov, and A. Sakamoto, Comprehensive study of Fröhlich polaron, Int. J. Mod. Phys. B **15**, 3940 (2001).

[15] K. Van Houcke, F. Werner, E. Kozik, N. Prokof'ev, B. Svistunov, M. J. H. Ku, A. T. Sommer, L. W. Cheuk, A. Schirotzek, and M. W. Zwierlein, Feynman diagrams versus Fermi-gas Feynman emulator, Nat. Phys. **8**, 366 (2012).

[16] W. Wu, M. Ferrero, A. Georges, and E. Kozik, Controlling Feynman diagrammatic expansions: Physical nature of the pseudogap in the two-dimensional Hubbard model, Phys. Rev. B **96**, 041105(R) (2017).

[17] R. Rossi, Determinant Diagrammatic Monte Carlo Algorithm in the Thermodynamic Limit, Phys. Rev. Lett. **119**, 045701 (2017).

[18] K. Chen and K. Haule, A combined variational and diagrammatic quantum Monte Carlo approach to the many-electron problem, Nat. Commun. **10**, 3725 (2019).

[19] C. Bertrand, O. Parcollet, A. Maillard, and X. Waintal, Quantum Monte Carlo algorithm for out-of-equilibrium Green's functions at long times, Phys. Rev. B **100**, 125129 (2019).

[20] A. Moutenet, P. Seth, M. Ferrero, and O. Parcollet, Cancellation of vacuum diagrams and the long-time limit in out-of-equilibrium diagrammatic quantum Monte Carlo, Phys. Rev. B **100**, 085125 (2019).

[21] R. Rossi, F. Simkovic, and M. Ferrero, Renormalized perturbation theory at large expansion orders, arXiv:2001.09133.

[22] J. Dick, F. Y. Kuo, and I. H. Sloan, High-dimensional integration: The quasi-Monte Carlo way, Acta Numer. **22**, 133 (2013).

[23] D. Nuyens, The construction of good lattice rules and polynomial lattice rules, arXiv:1308.3601.

[24] J. Dick and F. Pillichshammer, *Digital Nets and Sequences: Discrepancy Theory and Quasi-Monte Carlo Integration* (Cambridge University Press, Cambridge, 2010), https://doi.org/10.1017/CBO9780511761188.

[25] P. L'Ecuyer, Randomized quasi-Monte Carlo: An introduction for practitioners, in *Monte Carlo and Quasi-Monte Carlo Methods*, edited by A. B. Owen and P. W. Glynn (Springer International Publishing, Cham, 2018), pp. 29–52, https://link.springer.com/book/10.1007%2F978-3-319-91436-7.

[26] See Supplemental Material at http://link.aps.org/supplemental/10.1103/PhysRevLett.125.047702 for the details about calculation, error calculation in quasi-Monte Carlo methods, and properties and construction of the model function, which includes Refs. [27–46].

[27] K. F. Roth, On irregularities of distribution, Mathematika **1**, 73 (1954).

[28] H. Weyl, Über die Gleichverteilung von Zahlen Mod. Eins, Math. Ann. **77**, 313 (1916).

[29] N. M. Korobov, Approximate calculation of repeated integrals by number-theoretical methods, Dokl. Akad. Nauk SSSR **115**, 1062 (1957), http://www.mathnet.ru/php/archive.phtml?wshow=paper&jrnid=dan&paperid=22287&option_lang=eng.

[30] J. M. Hammersley, Monte Carlo methods for solving multivariable problems, Ann. N.Y. Acad. Sci. **86**, 844 (1960).

[31] J. C. van der Corput, Verteilungsfunktionen, Nederl. Akad. Wetensch. Proc. **38**, 813 (1935).

[32] J. H. Halton, On the efficiency of certain quasi-random sequences of points in evaluating multi-dimensional integrals, Numer. Math. **2**, 84 (1960).

[33] C. B. Haselgrove, A method for numerical integration, Math. Comput. **15**, 323 (1961).

[34] R. D. Richtmyer, The evaluation of definite integrals, and a quasi-Monte-Carlo method based on the properties of algebraic numbers, Technical Report No. LA-1342, Los Alamos Scientific Lab., Los Alamos, NM, 1952, https://dx.doi.org/10.2172/4405295.

[35] H. Niederreiter, Quasi-Monte Carlo methods and pseudo-random numbers, Bull. Am. Math. Soc. **84**, 957 (1978).

[36] H. Conroy, Molecular Schrödinger equation. VIII. A new method for the evaluation of multidimensional integrals, J. Chem. Phys. **47**, 5307 (1967).

[37] M. Berblinger and C. Schlier, Monte Carlo integration with quasi-random numbers: Some experience, Comput. Phys. Commun. **66**, 157 (1991).

[38] S. H. Paskov and J. F. Traub, Faster valuation of financial derivatives, J. Portfolio Manage. **22**, 113 (1995).

[39] X. Wang and I. H. Sloan, Why are high-dimensional finance problems often of low effective dimension?, SIAM J. Sci. Comput. **27**, 159 (2005).

[40] D. Nuyens and R. Cools, Fast algorithms for component-by-component construction of rank-1 lattice rules in shift-invariant reproducing kernel Hilbert spaces, Math. Comput. **75**, 903 (2006).

[41] G. P. Lepage, A new algorithm for adaptive multi-dimensional integration, J. Comput. Phys. **27**, 192 (1978).

[42] G. P. Lepage, VEGAS—An adaptive multi-dimensional integration program, Technical Report No. CLNS-447, Cornell Univ. Lab. Nucl. Stud., Ithaca, NY, 1980.

[43] A. N. Rubtsov and A. I. Lichtenstein, Continuous-time quantum Monte Carlo method for fermions: Beyond auxiliary field framework, J. Exp. Theor. Phys. Lett. **80**, 61 (2004).

[44] Y. Meir and N. S. Wingreen, Landauer Formula for the Current Through an Interacting Electron Region, Phys. Rev. Lett. **68**, 2512 (1992).

[45] P. B. Wiegmann and A. M. Tsvelick, Exact solution of the Anderson model: I, J. Phys. C **16**, 2281 (1983).

[46] B. Horvatić and V. Zlatić, Equivalence of the perturbative and Bethe-Ansatz solution of the symmetric Anderson Hamiltonian, J. Phys. France **46,** 1459 (1985).

[47] I. Sobol', On the distribution of points in a cube and the approximate evaluation of integrals, USSR Computational Mathematics and Mathematical Physics **7,** 86 (1967).

[48] F. Y. Kuo and D. Nuyens, Application of quasi-Monte Carlo methods to elliptic PDEs with random diffusion co-efficients: A survey of analysis and implementation, Found. Comput. Math. **16,** 1631 (2016).

[49] A. Tsvelick and P. Wiegmann, Exact results in the theory of magnetic alloys, Adv. Phys. **32,** 453 (1983).

[50] A. Okiji and N. Kawakami, Thermodynamic properties of the Anderson model (invited), J. Appl. Phys. **55,** 1931 (1984).

[51] S. J. Tans, M. H. Devoret, H. Dai, A. Thess, R. E. Smalley, L. J. Geerligs, and C. Dekker, Individual single-wall carbon nanotubes as quantum wires, Nature (London) **386,** 474 (1997).

[52] J. Nygård, D. H. Cobden, and P. E. Lindelof, Kondo physics in carbon nanotubes, Nature (London) **408,** 342 (2000).

[53] W. Liang, M. Bockrath, D. Bozovic, J. H. Hafner, M. Tinkham, and H. Park, Fabry—Perot interference in a nanotube electron waveguide, Nature (London) **411,** 665 (2001).

[54] N. Roch, S. Florens, V. Bouchiat, W. Wernsdorfer, and F. Balestro, Quantum phase transition in a single-molecule quantum dot, Nature (London) **453,** 633 (2008).

[55] M. Ridley, M. Galperin, E. Gull, and G. Cohen, Numerically exact full counting statistics of the energy current in the Kondo regime, Phys. Rev. B **100,** 165127 (2019).

[56] I. Krivenko, J. Kleinhenz, G. Cohen, and E. Gull, Dynamics of Kondo voltage splitting after a quantum quench, Phys. Rev. B **100,** 201104(R) (2019).

[57] C. W. J. Beenakker, Theory of Coulomb-blockade oscillations in the conductance of a quantum dot, Phys. Rev. B **44,** 1646 (1991).

[58] M. Hofheinz, X. Jehl, M. Sanquer, G. Molas, M. Vinet, and S. Deleonibus, Capacitance enhancement in Coulomb blockade tunnel barriers, Phys. Rev. B **75,** 235301 (2007).

[59] U. Schollwöck, The density-matrix renormalization group in the age of matrix product states, Ann. Phys. (Amsterdam) **326,** 96 (2011).

[60] I. Glasser, R. Sweke, N. Pancotti, J. Eisert, and J. I. Cirac, Expressive power of tensor-network factorizations for prob-abilistic modeling, with applications from hidden Markov models to quantum machine learning, arXiv:1907.03741.

[61] O. Parcollet, M. Ferrero, T. Ayral, H. Hafermann, I. Krivenko, L. Messio, and P. Seth, TRIQS: A toolbox for research on interacting quantum systems, Comput. Phys. Commun. **196,** 398 (2015).